ELSEVIER

Nuclear Physics A 581 (1995) 107–118

NUCLEAR PHYSICS A

Higher-order dynamical effects in Coulomb dissociation

H. Esbensen [a], G.F. Bertsch [b], C.A. Bertulani [c]

[a] *Physics Division, Argonne National Laboratory, Argonne, IL 60439, USA*

[b] *Institute of Nuclear Theory and Department of Physics, FM-15 University of Washington, Seattle, WA 98195, USA*

[c] *Gesellschaft für Schwerionenforschung, KPII, Planckstrasse 1, D-64291 Darmstadt, Germany*

Received 14 June 1994

Abstract

We study the effect of higher-order processes in Coulomb dissociation of ^{11}Li by numerically solving the three-dimensional time-dependent Schrödinger equation for the relative motion of a di-neutron and the ^{9}Li core. Comparisons are made to first-order perturbation theory and to measurements. The calculated Coulomb reacceleration effects improve the agreement with experiment, but some discrepancy remains. The effects are smaller in the dissociation of ^{11}Be, and they decrease with increasing beam energy.

1. Introduction

In recent years there has been several attempts to understand the effect of higher-order processes in Coulomb dissociation. The most recent activity [1–4] was spurred by three-body coincidence measurements [5] of the $^{11}\text{Li} \rightarrow {}^{9}\text{Li}+n+n$ breakup. It was observed that the average velocity of the charged fragment was larger than that of the two neutrons. This result may indicate that first-order perturbation theory is not sufficiently accurate to describe the dissociation of loosely bound nuclei. If that indeed is the case it would become very difficult to infer radiative capture rates from the inverse Coulomb dissociation measurements [6].

Previous studies of higher-order dynamical effects have not been very successful in describing the ^{11}Li data mentioned above. Due to the complexity of the problem it is customary to treat it as a two-body system consisting of a di-neutron interacting with the ^{9}Li core. Shyam et al. [1] made use of the post-representation form of the breakup process, and did not see any velocity shift of the charged fragment with respect to

SSDI 0375-9474(94)00423-4

the neutrons. Canto et al. [2] made coupled-channel calculations with a discretized continuum, including the dipole component of the Coulomb interaction with the target. They achieved some asymmetry in the relative velocity distribution, but not as much as seen in the experiment.

In the following we study the breakup using a simplified di-neutron model for ^{11}Li. We calculate the time evolution of the wave function for the relative motion of the core and the di-neutron in three dimensions. We calculate the momentum distributions for the breakup, and make comparisons to perturbation theory and to experimental data [5]. We also study the two-body breakup of ^{11}Be into a neutron and a ^{10}Be fragment.

The method we use is a straightforward generalization of the one- and two-dimensional calculations reported in Refs. [3,4]. An advantage of the method is that it is fairly easy to include higher multipole components of the Coulomb field. The quadrupole field is known to be important in the Barkas effect [7] in atomic stopping theory, and that motivated us to include it here.

2. Description of model calculations

We consider the breakup of a weakly bound projectile (Z_p, A_p), consisting of a tightly bound core (Z_c, A_c) and a cluster (Z_x, A_x),

$$(Z_p, A_p) \rightarrow (Z_c, A_c) + (Z_x, A_x),$$

due to the Coulomb interaction with a target nucleus (Z_t, A_t). We ignore for simplicity the scattering of projectile and target, and assume a straight-line trajectory for the relative motion, $\boldsymbol{R}(t) = \boldsymbol{b} - \boldsymbol{v}t$. The Coulomb field that excites the relative motion of the fragment and core is

$$V_{\mathrm{Coul}} = Z_t e^2 \left(\frac{Z_c}{|\boldsymbol{r}_{cp} - \boldsymbol{R}(t)|} + \frac{Z_x}{|\boldsymbol{r}_{xp} - \boldsymbol{R}(t)|} - \frac{Z_p}{R(t)} \right), \tag{1}$$

where $\boldsymbol{r}_{cp}$ and $\boldsymbol{r}_{xp}$ are the positions of the core and the cluster with respect to the center of mass of the projectile. It acts on the relative position $\boldsymbol{r} = \boldsymbol{r}_{xc}$ of the cluster and core through the transformations: $\boldsymbol{r}_{cp} = -\boldsymbol{r}A_x/A_p$ and $\boldsymbol{r}_{xp} = \boldsymbol{r}(1 - A_x/A_p)$. One can perform a multipole expansion of this interaction and for r_{cp} and r_{xp} smaller than $R(t)$ one can express the result in terms of a multipole-dependent effective charge,

$$e_\lambda = Z_c(-A_x/A_p)^\lambda + Z_x(1 - A_x/A_p)^\lambda. \tag{2}$$

We shall in particular consider the Coulomb dissociation of ^{11}Li into ^{9}Li and two neutrons, i.e. $Z_x = 0$ and $A_x = 2$. The dipole field dominates the breakup in this case, whereas the quadrupole field is less significant, partly due to a small effective charge. The quadrupole field would be relatively more important in dissociation of two charged fragments, as for example in the breakup of ^{8}B into a proton and ^{7}Be.

We adopt a simple di-neutron model for ^{11}Li and describe the ground state as an s-state bound by 0.3 MeV in a shallow Woods–Saxon potential, which has only one

bound state. The parameters of the potential is a depth of 6.57 MeV, a diffuseness of 0.67 fm and a radius of 2.496 fm. The time evolution of the wave function, in the presence of the Coulomb field from the target, is calculated using the method described in Ref. [4], generalized to a three-dimensional problem. The wave function is expanded in spherical harmonics,

$$\Psi(\boldsymbol{r},t) = \frac{1}{r}\sum_{\ell m} u_{\ell m}(r,t)Y_{\ell m}(\hat{r}), \tag{3}$$

and the source term S_m in Eq. (6) of Ref. [4] due to the Coulomb interaction with the target nucleus becomes

$$S_{\ell m}(r,t) = \sum_{\ell' m'}\langle Y_{\ell m}|V_{\rm Coul}|Y_{\ell' m'}\rangle u_{\ell' m'}(r,t). \tag{4}$$

We include all angular-momentum states up to $\ell = 8$, and $\lambda = 0$, 1 and 2 in the multipole expansion of the Coulomb field. We choose a coordinate system with a z-axis perpendicular to the reaction plane; the reflection symmetry in this plane implies that we only have to consider even values of $\lambda + \mu$ in the multipole expansion of the Coulomb field, and even values of $\ell + m$ in the wave function, since we start from an s-wave.

The reaction we want to study is the Coulomb dissociation of ^{11}Li on a lead target at a beam velocity of $v/c = 0.24$, corresponding to the experimental conditions of Ref. [5]. The ground-state wave function is represented on a radial grid which extends out to 150 fm in steps of 0.2 fm. We start the dynamical calculation at $t_{\rm i} = -1000$ fm/c at which time the distance between projectile and target is larger than the adiabatic distance, $\hbar v/\Delta E$, even for excitations near threshold ($\Delta E t_{\rm i}/\hbar = 1.5$ for $\Delta E = 0.3$ MeV). We follow the time-evolution in steps of 2 fm/c up to $t_{\rm f} = +1000$ to 3000 fm/c, depending on the impact parameter. The decision to stop the calculation is determined by several requirements which must be met to obtain a reliable momentum distribution. First of all, the dissociation probability must have converged. Secondly, the continuum part of the wave function must have left the potential well but it must not yet have reached the outer boundary of the radial grid. Finally, the long-range influence of the Coulomb field, after we stop the calculation, should not be too significant.

From the final wave function, $\Psi(t_{\rm f})$, obtained for a given impact parameter b, we calculate the dissociation or breakup probability as

$$P_{\rm diss}(b) = 1 - |\langle\Psi_{\rm gs}|\Psi(t_{\rm f})\rangle|^2, \tag{5}$$

where $\Psi_{\rm gs}$ is the ground-state wave function. As in Ref. [4], we extract the continuum part of the final wave function,

$$\Psi_{\rm cont}(t_{\rm f}) = \Psi(t_{\rm f}) - \Psi_{\rm gs}\langle\Psi_{\rm gs}|\Psi(t_{\rm f})\rangle, \tag{6}$$

and project out the momentum distribution,

$$\frac{{\rm d}P(\boldsymbol{p},b)}{{\rm d}\boldsymbol{p}} = |\langle\boldsymbol{p}|\Psi(t_{\rm f})\rangle|^2. \tag{7}$$

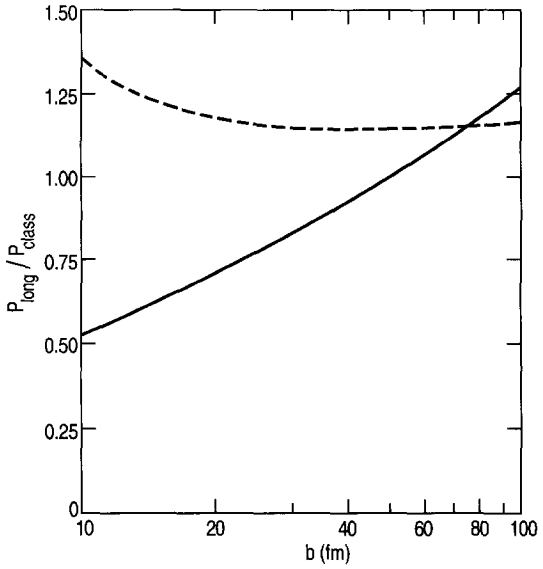

Fig. 1. Impact-parameter dependence of the average longitudinal (solid curve) and transverse momenta (dashed curve) for the relative motion of the di-neutron and ^{9}Li after Coulomb dissociation, in units of p_{class} defined in Eq. (8).

The normalization of this distribution is the breakup probability. The differential cross sections discussed in the next section are then obtained by integrating over an appropriate range of impact parameters.

Of particular interest is the average momentum of this wave function. In first-order perturbation theory this would be zero. In a simple picture one might expect that the dissociation takes place essentially at $t = 0$ and the continuum wave function would then acquire the classical, longitudinal momentum

$$p_{class} = Z_t(Z_x - Z_p A_x/A_p)e^2/vb \tag{8}$$

along the beam direction, where $(Z_x - Z_p A_x/A_p)$ is the dipole effective charge associated with the projectile wave function. We find it instructive to present the average longitudinal momentum in units of this simple estimate. The result we obtain is shown as a function of impact parameter by the fully drawn curve [1] in Fig. 1. The longitudinal momentum is seen to be reduced compared to the simple classical estimate at the smaller impact parameters but it reaches this value at about 50 fm. We also show as the dashed curve in Fig. 1 the average transverse momentum in the reaction plane, perpendicular to the beam direction. It decreases slightly for increasing impact parameters and is larger than the classical value (8).

[1] The longitudinal momentum has been corrected for the long-range Coulomb acceleration that occurs after the time we stop the numerical calculation. The correction amounts to at most 5% of p_{class}.

3. Comparisons to perturbation theory

The calculated dipole response from the di-neutron ground state is shown in Fig. 2 as a function of the excitation energy. It peaks at 0.48 MeV, and the total strength, $B(\mathrm{E1}) = 2.5\ e^2\mathrm{fm}^2$. This is about 67% larger than the prediction of the di-neutron model based on a zero-range nuclear binding potential [8], but the overall shapes are quite similar.

In first-order perturbation theory, the excitation probability is given by the expression,

$$P_{\mathrm{fop}}(b) = \frac{4\pi}{9}\left(\frac{2Z_t e^2}{\hbar w}\right)^2 \int_0^\infty \mathrm{d}E_c \frac{\mathrm{d}B(\mathrm{E1})}{\mathrm{d}E}\frac{\xi^2}{b^2}\left(K_0^2(\xi) + K_1^2(\xi)\right), \tag{9}$$

where $\xi = \Delta E b/\hbar w$ and $\Delta E = E_c + |E_{\mathrm{gs}}|$ is the excitation energy; see Ref. [9] for a review. Note that we have not included relativistic effects in our calculations. This probability is meaningful only if it is small compared to unity. However, since it can become quite large as shown by the dashed curve in Fig. 3, it is more reasonable to use the following prescription for the breakup or dissociation probability:

$$P_{\mathrm{diss}}(b) = 1 - \exp(-P_{\mathrm{fop}}(b)), \tag{10}$$

which is the result one obtains for a coherent state, taking into account the effect of multiple excitations. This result is shown by the fully drawn curve in Fig. 3, and it compares quite well with the results of the dynamical calculations discussed in the previous section, which are shown by the open circles. The largest deviation in this

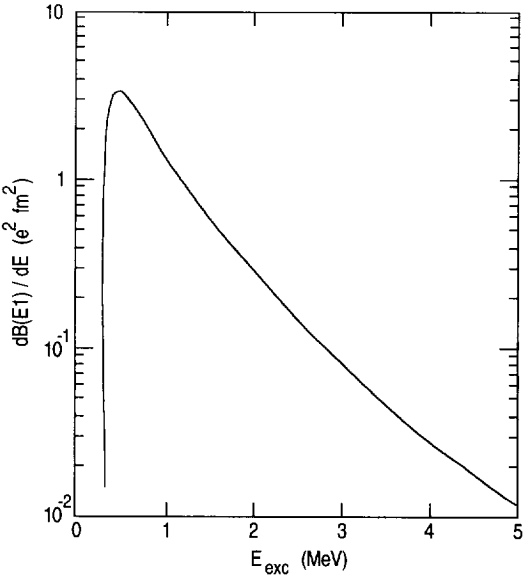

Fig. 2. Dipole response from the di-neutron ground state in ^{11}Li as a function of excitation energy. The threshold is located at 0.3 MeV.

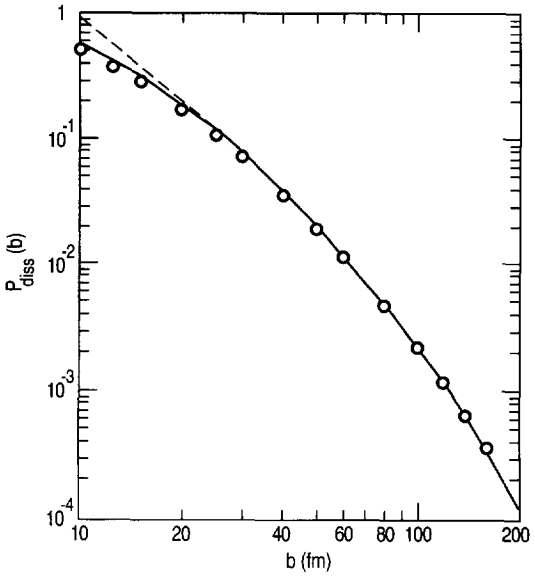

Fig. 3. Coulomb dissociation probabilities as functions of impact parameter. The open circles are the results of the dynamical calculations discussed in the text. The dashed curve is the result obtained in first-order perturbation theory (Eq. (7)), and the fully drawn curve is the result obtained from Eqs. (9) and (10).

figure is 15% and appears at 10 fm. The almost perfect agreement at large impact parameters is actually a good check on the dynamical calculations.

In practical calculations of dissociation cross sections there are of course several uncertainties and corrections which set in at the smallest impact parameters, such as the nuclear dissociation and absorption and corrections for Coulomb trajectories. If we more or less arbitrarily choose an impact parameter range of $11 \leqslant b \leqslant 160$ fm, which we have covered by the dynamical calculations, we obtain a cross section of 8 b. The result obtained from the fully drawn curve is only 6% higher, whereas the result obtained from the dashed curve is 16% higher. Thus it appears that one can obtain quite reliable cross sections from first-order perturbation theory using the prescription Eq. (10), and there does not appear to be an urgent need for doing full dynamical calculations.

Let us mention that our di-neutron model is somewhat unrealistic: the total dipole strength and the Coulomb dissociation cross section are about a factor of two larger than more realistic estimates, see for example Refs. [5,10]. A way to fix this discrepancy is to reduce the effective charge by a factor of 0.7. The direct coupling between the ground state and the continuum would then be realistic, but the continuum–continuum coupling would become too weak. We have therefore decided not to make any adjustments of our model at this point, since the main purpose of our study is to see the effect of continuum–continuum couplings.

In first-order perturbation theory, the momentum distribution generated by dipole excitations from the spherical ground state is

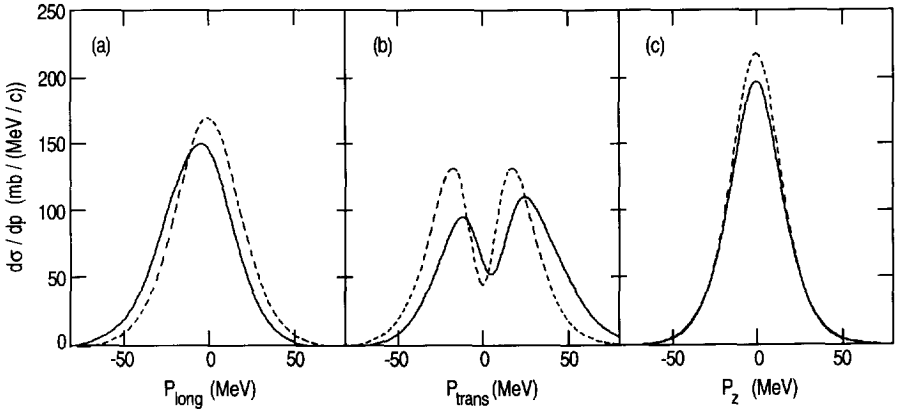

Fig. 4. The three projections of the momentum distribution for the relative motion of the di-neutron and the ^{9}Li core after Coulomb dissociation, viz. the longitudinal (a), the transverse in the reaction plane (b) and the out-of-plane projection (c) on the z-axis, which is perpendicular to the reaction plane. The dashed curves are based on first-order perturbation theory, and the solid curves are the results of the dynamical calculations discussed in the text.

$$\frac{\mathrm{d}P_{\mathrm{fop}}(\boldsymbol{p},b)}{\mathrm{d}\boldsymbol{p}} = \frac{1}{3}\left(\frac{2Z_{\mathrm{t}}e^2}{\hbar w}\right)^2 \frac{\mathrm{d}B(\mathrm{E1})}{p^2\,\mathrm{d}p}\frac{\xi^2}{b^2} \times \left(K_0^2(\xi)\cos^2(\theta_{p,\ell}) + K_1^2(\xi)\cos^2(\theta_{p,\mathrm{t}})\right), \tag{11}$$

where the $\theta_{p,\ell}$ and $\theta_{p,\mathrm{t}}$ are the angles between the momentum $\boldsymbol{p}$ and the longitudinal and transverse directions, respectively. We shall always normalize this distribution according to Eq. (10). We first examine the three projections of this distribution, namely the longitudinal (along the beam axis), the transverse (perpendicular to the beam and in the scattering plane), and finally the projection on the z-axis perpendicular to the scattering plane. A characteristic feature at intermediate and high beam energies is the dominance of transverse dipole excitations (the last term in Eq. (11)) over longitudinal dipole excitations (the first term). From the simple $\cos(\theta)$ dependence in Eq. (11) it is then seen that the transverse-momentum distribution will have a local minimum for p_{trans} =0, whereas the longitudinal and the out-of-plane distributions will have a maximum at zero, and the out-of-plane distribution will be the narrower.

The momentum distributions for the relative motion of the di-neutron and the ^{9}Li core that we obtain are shown in Fig. 4 together with the results of perturbation theory (dashed curves). The differential cross sections were obtained by integrating over the impact parameter range $11 \leqslant b \leqslant 160$ fm. The longitudinal distribution (a) is found to be shifted compared to the symmetric prediction of first-order perturbation theory, with an average shift of -7 MeV/c. The effect is somewhat larger on the in-plane transverse-momentum distribution (b), where the average shift is 12 MeV. Finally, the out-of-plane distribution (c) is rather insensitive to higher-order dynamical effects.

4. Comparisons to measurements

We now compare the calculations to the measurements of Ref. [5]. Using the coincident measurement of the momenta of the three particles in the final state, this experiment inferred the ^{11}Li decay energy spectrum and the distribution in the difference of velocities between the ^{9}Li and the neutron pair. Unfortunately, due to a limited acceptance in the experiment, it is not completely trivial to compare with theory.

We first consider the decay energy spectrum. Experimentally, this is the distribution of energies of the final-state particles in their center-of-mass system. In our di-neutron model, the decay energy is related to the momentum of the final-state wave function by $E_{\rm dec} = p^2/2\mu_{\rm xc}$, where $\mu_{\rm xc} = m_{\rm n}A_{\rm x}(A_{\rm p} - A_{\rm x})/A_{\rm p}$. In Fig. 5 we show the theoretical distributions obtained in perturbation theory (dashed line) and with higher-order dynamic effects (solid line). Also shown are the data (with an arbitrary normalization) obtained in Ref. [5] and corrected for the detection efficiency (Fig. 11 of Ref. [5]). Although our di-neutron model does not account for the shape of the measured spectrum at small excitation energies, the discrepancy between our two numerical results clearly indicate that one cannot extract the dipole response directly from the measurement and the equivalent photon spectrum, i.e. by assuming first-order perturbation theory to be valid.

We next consider the distribution in the longitudinal velocity, which is very sensitive to Coulomb reacceleration. The average longitudinal velocity for the relative motion of

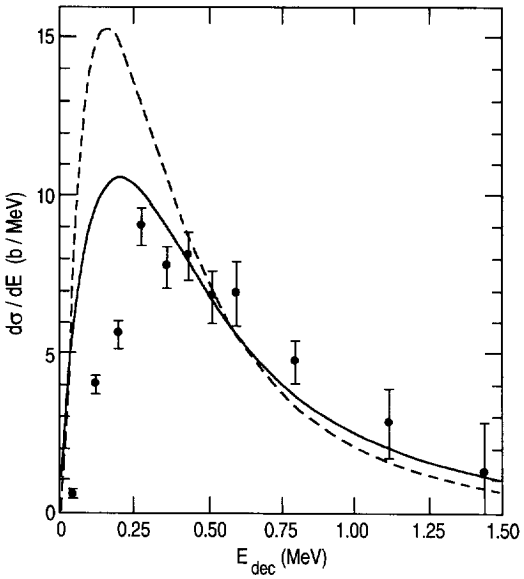

Fig. 5. Decay energy spectrum for ^{11}Li after Coulomb dissociation on a lead target at 28 MeV/A, obtained in first-order perturbation theory (dashed curve) and from the dynamical calculations discussed in the text (solid curve). Also shown are the experimental results [5] (with an arbitrary normalization), which have been corrected for the detection efficiency.

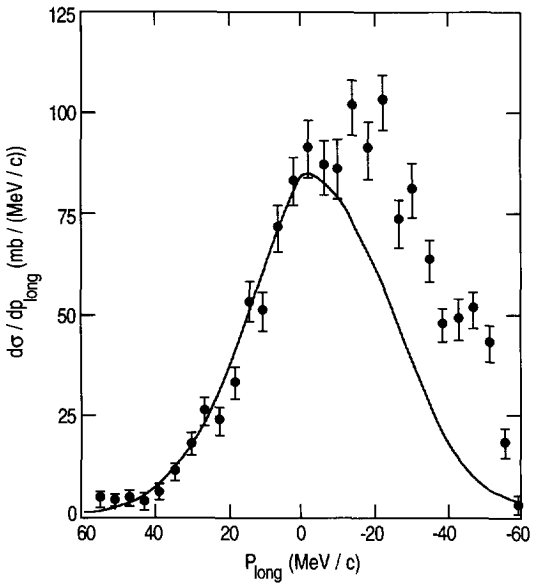

Fig. 6. "Longitudinal" momentum distribution for the relative motion of the di-neutron and the ^{9}Li core. The experimental results [5] have not been corrected for detection efficiency. The calculated curve include the effect of Coulomb deflection and the finite acceptance angle of the neutron detectors.

the ^{9}Li fragment and the two neutrons is calculated to be $\delta v/c = +0.005$, using the results shown in Fig. 1. This is comparable to, but somewhat smaller than the measured value [5] of +0.008.

The experiment provides detailed information about the distribution with a graph of the spectrum as a function of the difference in speeds (velocity magnitudes) between the ^{9}Li and the neutron pair, Fig. 14 in Ref. [5]. The speed difference can be written as

$$\Delta v = |\boldsymbol{v}_{\mathrm{f,cm}} + \boldsymbol{v}_9| - |\boldsymbol{v}_{\mathrm{f,cm}} + \boldsymbol{v}_{2\mathrm{n}}|, \tag{12}$$

where $v_{\mathrm{f,cm}}$ is the center-of-mass velocity of the three fragments in the laboratory system, and v_9 and $v_{2\mathrm{n}}$ are the velocities of ^{9}Li and the two neutrons, respectively, in the rest frame of the three-body system. To second order in the relative velocity we obtain

$$\Delta v = \left((\boldsymbol{v}_9 - \boldsymbol{v}_{2\mathrm{n}}) \cdot \boldsymbol{v}_{\mathrm{f,cm}} - \tfrac{7}{22}|\boldsymbol{v}_9 - \boldsymbol{v}_{2\mathrm{n}}|^2\right) / v_{\mathrm{f,cm}}. \tag{13}$$

The first term is the relative velocity measured along the direction of the final center-of-mass motion, and the last term is a small correction that we can ignore.

The experimental and calculated distributions are shown in Fig. 6. For the calculated distribution, the internal momentum distribution is projected onto the direction of the final center-of-mass motion for each impact parameter, and then an appropriate average is taken over impact parameters. Here we have also included the corrections for the small acceptance angle of the neutron detectors, which have an opening angle of about 5°. Roughly speaking, this implies the elimination of events which have a transverse

momentum ($\sqrt{p_{\rm trans}^2 + p_z^2}$) larger than 32 MeV/$c$. This is quite a significant cut as can be seen in Fig. 4, and it will, in particular, reduce the relative contribution from small impact parameters, where we obtain the broadest momentum distributions and where the higher-order dynamical effects (including Coulomb deflection) are the largest. The cut reduces the calculated cross section to about 50% of its original value.

The calculated distribution shown in Fig. 6 reproduces the data quite well at positive "longitudinal" momenta and shows some asymmetry, but not enough to reproduce the data at the largest negative momenta. Our results are similar to those obtained by Canto et al. [2], who only made use of the dipole field. The point is that the dipole field plays the dominant role, whereas the effect of the monopole and quadrupole fields is rather insignificant in our calculations. Let us finally mention that there are additional corrections to consider (for example energy loss in target, energy dependence of neutron-detection efficiency) before one can make definitive conclusions from the comparison to the data. We have chosen not to pursue such corrections any further at this point. New measurements, which cover a much larger neutron acceptance angle, will hopefully become available in the future.

We finally study the Coulomb dissociation of ^{11}Be into a neutron and a ^{10}Be fragment, which has recently been measured at 72 MeV/A on a lead target [11]. The analysis of the data showed good agreement with the semiclassical model of Ref. [12]. Here we shall again compare the data to first-order perturbation theory and to higher-order dynamical calculations.

We use a potential model for ^{11}Be assuming an inert ^{10}Be core plus a valence neutron. A Woods–Saxon potential is used with parameters $V_0 = -51.55$ fm, $R = 3$ fm, and $a_0 = 0.52$ fm. These parameters reproduce the $2s_{1/2}$ ground-state binding energy of 0.505 MeV. The differential cross section was calculated in first-order perturbation theory, and it was normalized so that good agreement with the experimental data was found (dashed line in Fig. 7a). This required a scaling factor 0.87, which is somewhat larger than the spectroscopic factor of 0.77 deduced from the ^{10}Be(d,p)^{11}Be reaction [13]. The agreement with the experimental data is very good in view of the simplicity of the model. Indeed, as discussed by Nakamura et al. [11], the Coulomb breakup of this halo nucleus is primarily sensitive to the tail of the valence-neutron wave function, which has a simple Yukawa form. A similar conclusion was reached by Anne et al. [14] from an analysis of the angular distribution of the emitted neutrons.

Starting from the $2s_{1/2}$ ground state the effects of Coulomb reacceleration were calculated. The results of the non-perturbative calculation is given by the solid line in Fig. 7a, with the same normalization factor. We see that the reacceleration effect causes a very slight modification of the energy spectrum.

We have repeated the calculations at a smaller beam energy of 28 MeV/A. The results are shown in Fig. 7b. We see that the reacceleration effect is much larger, although not as large as in the ^{11}Li case (compare Figs. 5 and 7b). This shows that the reacceleration effect is dependent on the breakup probabilities. The breakup probability of ^{11}Be is about a factor 2 smaller than that of ^{11}Li, essentially because the effective dipole charge

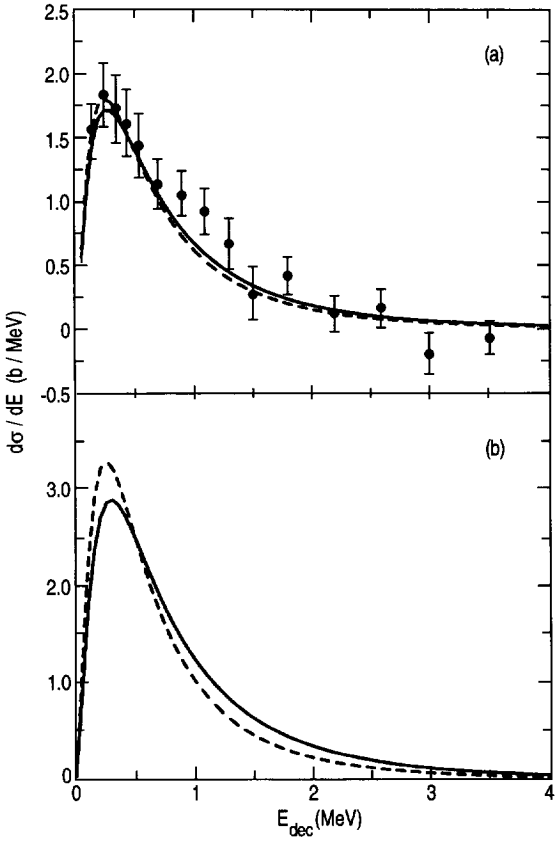

Fig. 7. Energy spectrum for the dissociation of ^{11}Be projectiles on a lead target at 72 MeV/A is shown in (a). The dashed curve is the prediction of first-order perturbation theory normalized to the data points [11]. The solid curve is obtained by the numerical solution of the Schrödinger equation. Similar results are shown in (b) for a beam energy of 28 MeV/A.

is a factor of 1.5 smaller. The effect is also dependent on the bombarding energy, being smaller at larger beam energies. This occurs because the breakup probability decreases with increasing beam energy in this energy interval, cf. Eq. (9).

5. Conclusions

Our study of higher-order processes in Coulomb dissociation in a three-dimensional model confirms the general behavior of the Coulomb reacceleration found in an earlier one-dimensional study [3]. When the excited state is not a very narrow resonance, the magnitude of the reacceleration is similar to the classical value assuming an instantaneous breakup at the distance of closest approach. This is unfortunate for using the reaction to measure low-energy transition strengths, because reacceleration effects distort the sought spectrum.

In the case of ^{11}Li, we found severe distortion of the spectrum for the energy region at and below the peak. On the other hand, the distortion was small on the high-energy side of the peak, so a simple analysis could be used confidently there. Canto et al. [2] have studied ^{11}Li Coulomb dissociation with a model including the same physics, but using a different numerical method. They also find substantial distortion of the excitation energy spectrum in the peak region, but practically no effect of the higher-order interactions above 0.6 MeV.

The data on the relative velocity of the ^{9}Li fragment and the two neutrons is more problematic. Our predicted distribution is not skewed as much as the experimental distribution toward the side of a faster ^{9}Li. We fit the distribution on the slower side but not on the faster side. In this we agree with the calculation of Ref. [2]. However, additional corrections associated with the experimental conditions may affect the distribution, so we do not wish to make a firm conclusion on the basis of this comparison.

It is clear that Coulomb reacceleration effects are significant in the dissociation of ^{11}Li, and they can qualitatively be accounted for in the di-neutron model. The lack of quantitative agreement is certainly not a failure of the numerical techniques, but the basic model assumption of a two-body system is questionable. On the other hand, Coulomb dissociation of ^{11}Li at a moderate beam energy is probably one of the most dramatic cases concerning effects of higher-order dynamical processes. The effects are smaller for ^{11}Be. Moreover, they decrease with increasing beam energy. The latter fact must clearly be considered in the planning of future measurements.

Acknowledgements

This work was supported by the US Department of Energy, Nuclear Physics Division, under Contracts W-31-109-ENG-38 and FG-06-90ER-40561.

References

[1] R. Shyam, P. Banerjee and G. Baur, Nucl. Phys. A 540 (1992) 341.
[2] L.F. Canto, R. Donangelo, A. Romanelli and H. Schulz, Phys. Lett. B 318 (1993) 415.
[3] G.F. Bertsch and C.A. Bertulani, Nucl. Phys. A 556 (1993) 136.
[4] C.A. Bertulani and G.F. Bertsch, Phys. Rev. C 49 (1994) 2839.
[5] D. Sackett et al., Phys. Rev. C 48 (1993) 118.
[6] G. Baur, C.A. Bertulani and H. Rebel, Nucl. Phys. A 458 (1986) 188.
[7] J. Lindhard, Nucl. Instr. Meth. 132 (1976) 1.
[8] C.A. Bertulani, G. Baur and M.S. Hussein, Nucl. Phys. A 526 (1991) 751.
[9] C.A. Bertulani and G. Baur, Phys. Reports 163 (1988) 299.
[10] H. Esbensen, G.F. Bertsch and K. Ieki, Phys. Rev. C 48 (1993) 326.
[11] T. Nakamura et al., Phys. Lett. B 331 (1994) 296.
[12] G. Baur, C.A. Baur and D. Kalassa, Nucl. Phys. A 550 (1992) 527.
[13] B. Zwieglinski et al., Nucl. Phys. A 315 (1979) 124.
[14] R. Anne et al., Phys. Lett. B 304 (1993) 55.